A different approach for determining the responsivity of n^+p detectors using scanning electron microscopy

Omeime Xerviar Esebamen†, Göran Thungström, and Hans-Erik Nilsson

Department of Information Technology and Media, Mid Sweden University, Holmgatan 10, SE-851 70, Sundsvall, Sweden

Abstract: This paper explores an alternative to the standard method of studying the responsivities (the input–output gain) and other behaviours of detectors at low electron energy. The research does not aim to compare the results of differently doped n^+p detectors; its purpose is to provide an alternative characterization method (using scanning electron microscopy) to those used in previous studies on the responsivity of n^+p doped detectors as a function of the electron radiation energy and other interface parameters.

Key words: scanning electron microscopy; responsivity; n^+p detector

DOI: 10.1088/1674-4926/33/7/074002 **EEACC:** 2520

1. Introduction

In semiconductor solid state physics, carrier generation and recombination are processes by which mobile charge carriers (electrons and electron holes) are created and annihilated. Carrier generation and recombination processes are indispensable to the application in many optoelectronic semiconductor devices, such as photodiodes, LEDs and laser diodes. Irradiation of a detector results in the formation of electron–hole pairs which is the fundamental unit of generation and recombination, corresponding to an electron transitioning between the valence band and the conduction band.

Any defect or impurity at the surface of the semiconductor encourages recombination and the rate at which such recombination of carriers takes place is determined by the electron and hole concentrations, the band structure of the semiconductor and the electronic properties of the defect at the Si–SiO_2 interface[1]. As the surface of a detector suffers a severe disturbance of the crystal lattice, this area of the detector is a major center of particularly high recombination[2]. A well known fact is that the high recombination rate in the proximity of a surface diminishes the concentration of minority carriers in this region. It has a harmful effect on the short-circuit current since the top surface also amounts to the highest generation region of carriers in the radiation detector[3].

At the interface of the semiconductor (Si–SiO_2 interface), the expression for the velocity at which the minority carriers recombine is similar to the low injection bulk-recombination process in which the minority carrier lifetime τ is equal to $(\sigma_p v_{th} N_{st})^{-1}$. In an n-type material, the interface recombination velocity of minority carriers S_p is depicted as

$$S_p = \sigma_p v_{th} N'_{st}, \quad (1)$$

where σ_p represents the hole capture cross section; v_{th}, the thermal velocity; and N'_{st} represents the number of trap centers (energy levels) per unit area[3].

In order to lower the interface recombination of minority carriers which studies have shown can have a major effect on the short-circuit current, the open-circuit voltage and the responsivity of the detector, the amount of dangling silicon bonds at the top surface is minimised by growing a layer of silicon dioxide, SiO_2 on the top surface of the detector. Although it helps to solve the problem described above, the growth of SiO_2 on the silicon wafer introduces other phenomena known as trapped charges; one of which is the oxide fixed charge Q_f. Q_f, otherwise regarded as charge sheet, is located within approximately 3 nm of the Si–SiO_2 interface and is associated with defects in SiO_2. It is also fixed and very challenging to charge or discharge. A typical Q_f for a well prepared Si–SiO_2 interface is approximately 10^{10} cm^{-2} for a $\langle 100 \rangle$ silicon surface, and about 5×10^{10} cm^{-2} for a $\langle 111 \rangle$ silicon surface[4].

There are a number of methods for measuring detector responsivity. One very popular technique is the photoconductance method[5, 6]. Another method involves the use of the microscope's electron beam to generate an induced current in order to map the electronic activity of the test sample, among other things, and is known as electron beam induced current (EBIC)[7, 8]. While these methods are well known and effective, they come with the added task of using electronic components and equipment[9]. For example, while the photoconductance method requires good optical detectors for measuring optical power, as well as the use of a lock-in amplifier, the EBIC method requires the use of the additional parts of a typical EBIC system. These consists of an external low-noise current amplifier located outside the SEM's high-vacuum chamber, a signal conditioning circuit, and a high-vacuum electrical feed-through to act as a bridge between the external current amplifier and the sample inside the SEM chamber.

As a result, the benefit of the method used in this report is that the use of external electronics is minimal. We have investigated different n^+p detectors and the effect on the responsivity of the detector when implanted with different donors at low energy. Also investigated was the consequence of Q_f on the detector's responsivity as well as its net recombination when irradiated with electrons.

† Corresponding author. Email: Omeime.esebamen@miun.se
Received 27 January 2012, revised manuscript received 9 March 2012
© 2012 Chinese Institute of Electronics

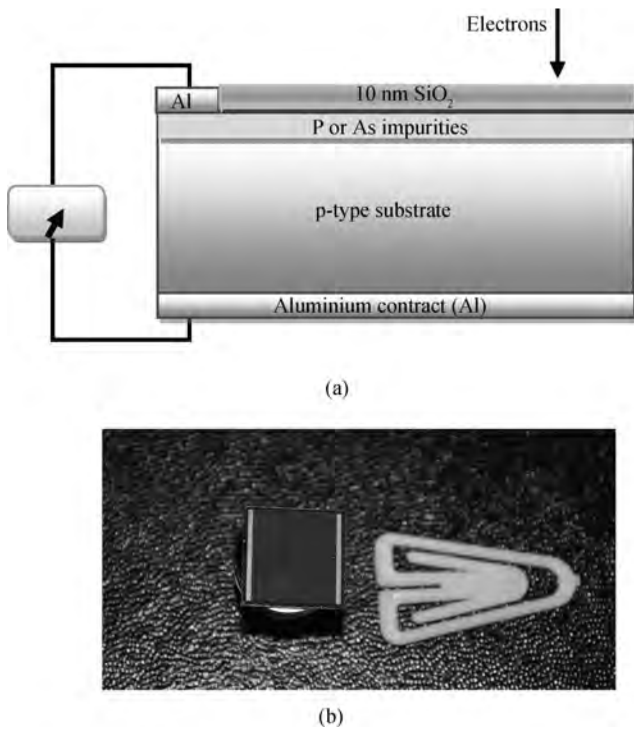

Fig. 1. (a) Schematic of the simulated n^+p detectors (not drawn to proportion) and the electron beam illumination spot. (b) Image of the fabricated detector.

Table 1. Parameter used for the simulation process of the detectors. Simulation of all the processing steps as well as the implantation of impurities through 570 Å thick SiO_2 were done to mimic the processing described in the fabrication process in the next sub-section.

Implantation		
Dopant	Dose (cm^{-2})	Energy (keV)
Phosphorus	0.4×10^{15}	30
Arsenic	0.4×10^{15}	56.4
Diffusion (Phosphorus and arsenic)		
Temperature (℃)	Time (min)	Anneal gas
900	30	Nitrogen

2. Simulation methodology and experimental process

2.1. Simulation procedures

In order to identify the effects of the aforementioned surface states on the detector operation, two n^+p detectors with different impurity dopants (arsenic and phosphorus) and distribution were simulated. Both detectors were simulated using the same processing methods shown in Table 1. A schematic of the simulated n^+p detector is shown in Fig. 1(a) while the concentration diffusion profile and resultant electric field of the detectors are shown in Fig. 2.

To model the interaction between the electrons and the detector, Monte Carlo (MC) simulation methods of Geant4 and Taurus Medici were used. "Standard" electromagnetic processes were employed from the former to track the passage of bombarding electron particles through the detector taking into

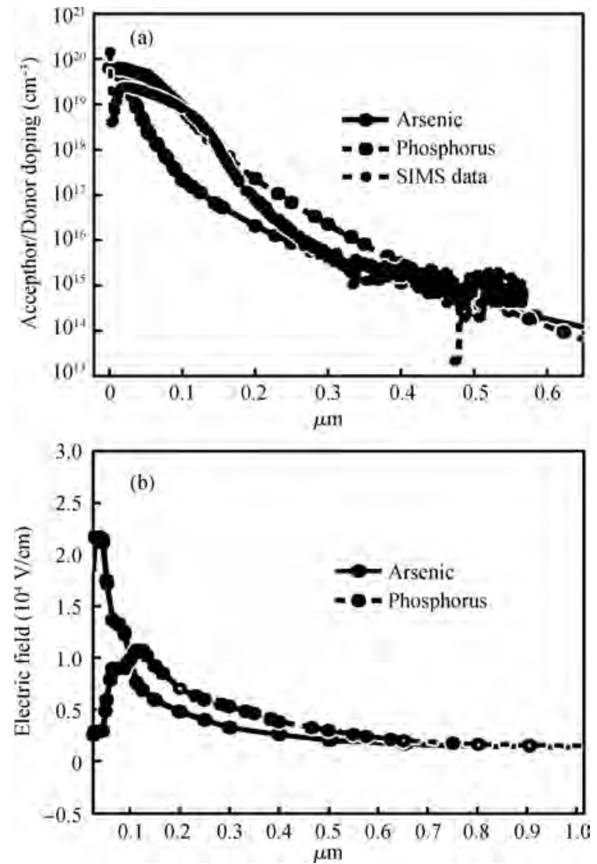

Fig. 2. (a) The simulated phosphorus and arsenic concentration diffusion profile of the detectors. (b) Electric field created by the doping gradient. As a result of the deeper arsenic profile, the built-in electric field is higher and as such of more effective movement of holes into the depletion layer compared to the weaker electric field of the phosphorus profile.

account possible interactions and decay processes[1] [10]. To analyze the silicon bulk and the Si–SiO_2 interface, we used some simple mobility models in Taurus Medici such as the parameterization of mobility model to account for carrier heating and velocity saturation effects[11, 12]. At every point on the discrete mesh of the Si–SiO_2 interface, a simple model used during the simulation by which an effective Shockley–Read–Hall (SRH) recombination lifetime for each carrier τ_n^{eff} was related to the recombination velocities of electrons S_p by

$$\frac{1}{\tau_n^{eff}(i)} = \frac{S_p d_i}{A_i} + \frac{1}{\tau_p(i)}, \tag{2}$$

where $\tau_p(i)$ is the SRH lifetimes that are trap-assisted recombination lifetime (concentration dependent), A_i the semiconductor area associated with the node; and d_i, the length of the interface associated with the node[2].

[1] Geant4 employs an aggregate of the composition and rejection Monte Carlo methods and comes with facilities for handling geometry, tracking, detector response, run management, visualization and user interface.

[2] Every region of the device structure is divided into a mesh of nonoverlapping triangular elements. Solution values during simulations are calculated at the mesh nodes at the corners of the triangular elements. The total number of nodes in an interface region is calcu-

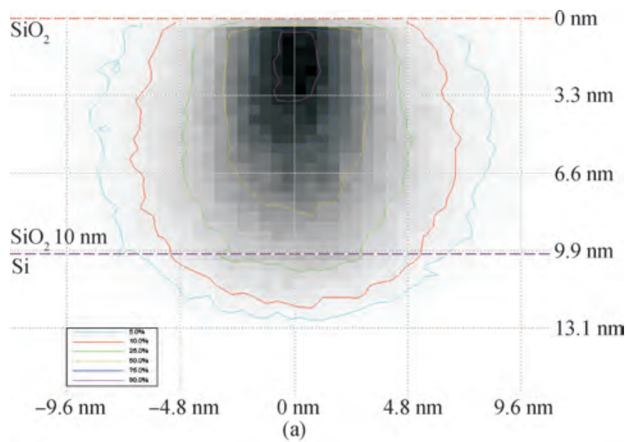

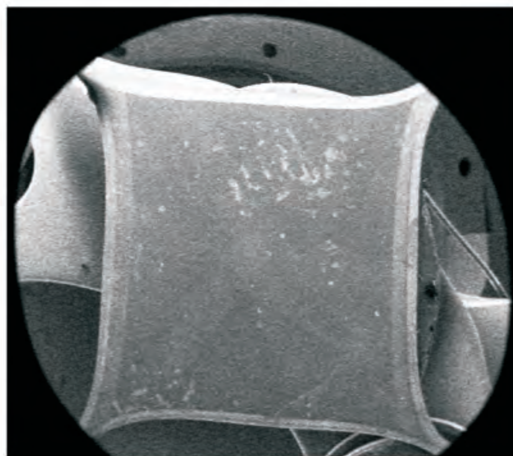

Fig. 3. Energy by position diagram showing the cross-sectional perspective of absorbed energy (by position) in the detector substrate with 10 nm SiO_2 passivation layer simulated at 0.5 keV, 200 000 electron trajectories with a beam radius of 10 nm. It shows the display of energy contour lines calculated from the center of the electron imping-ing point and shows the percentage of energy not contained within the line. For example, a 10% line is the frontier between an area containing 90% of the absorbed energy and the rest of the sample (b). A scanning electron microscope low magnification image of the fabricated detector obtained with 15 keV primary electrons by the Stereoscan 360. The detector has a dimension of 12mm by 12mm.

Using the Monte Carlo simulation tool CASINO v2.42, the cross-sectional perspective of the absorbed energy (by position) in the detector substrate with a 10 nm SiO_2 passivation layer is simulated at 0.5 keV, with 200 000 electron trajectories, as shown in Fig. 3(a). From the diagram, the gray shading overlay ranges from light to dark as the density of absorbed energy increases[3]. It is seen that though a major part of the energy is absorbed by the passivating oxide, an appreciable amount of electrical output greater than the detector dark current can still be generated from the absorbed energy in the active layer.

lated by adding the number of mesh points in the region, plus the number of mesh points along exposed boundaries[6].

[3]These tools (Geant4 and CASINO) were used because they are specifically designed for low energy beam interaction and can be used to generate many of the recorded signals (X-rays and backscattered electrons) in a scanning electron microscope (SEM) as well as to simulate enough electron trajectories to represent the condition used to image semiconductor structures in a SEM.

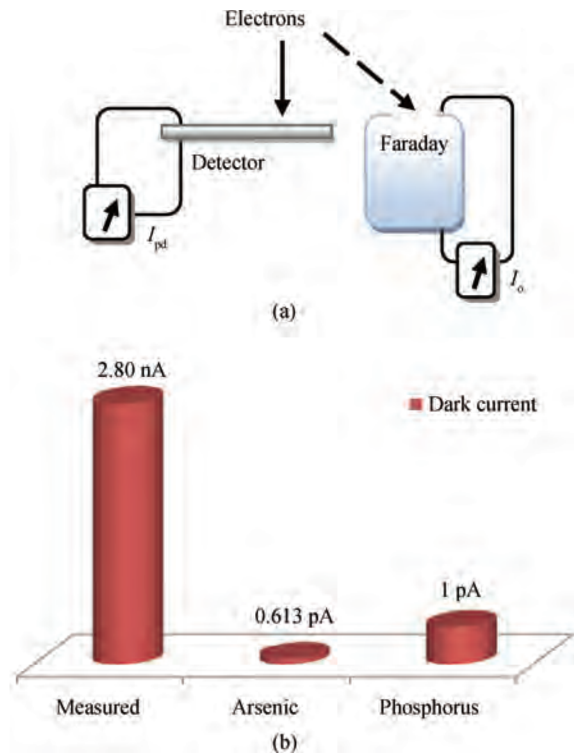

Fig. 4. (a) Experimental setup to measure electron beam current. (b) The measured leakage current of the detector in comparison with the simulated detectors at 2.5 V.

2.2. Fabrication process

A detector was fabricated at the Mid Sweden University cleanroom using the parameters associated with the detector doped with arsenic dopant in Table 1 on a 403 μm thick p-type silicon wafer of $\langle\overline{111}\rangle$ orientation and axial resistivity of 4.15 kΩ·cm when measured by the 2-point method. Boron was first slowly diffused into the wafer as substrate doping through a thin layer of thermally grown oxide. After the necessary photolithographic processes for mask and pattern transfer, a precisely controlled amount of low-energy dopant impurity was implanted into the top region of the silicon material through 570 Å thick SiO_2 which was etched away after the implantation. Then, a high-temperature drive-in step at 900 ℃ through diffusion process for 30 min formed the n-type buried layer. Finally, aluminum of about 500 Å thickness was deposited as front and back ohmic contacts. While wet chemical etching was employed at every etching stage, care was taken to avoid any contaminants on the surface of the device since the state of the detector's interface(s) were of utmost importance[13].

3. Analyses and results

3.1. Measurement

Scanning electron microscope (Stereoscan 360) was used for measurements and the detector current measured at a particular energy was used to calculate the measured responsivi-

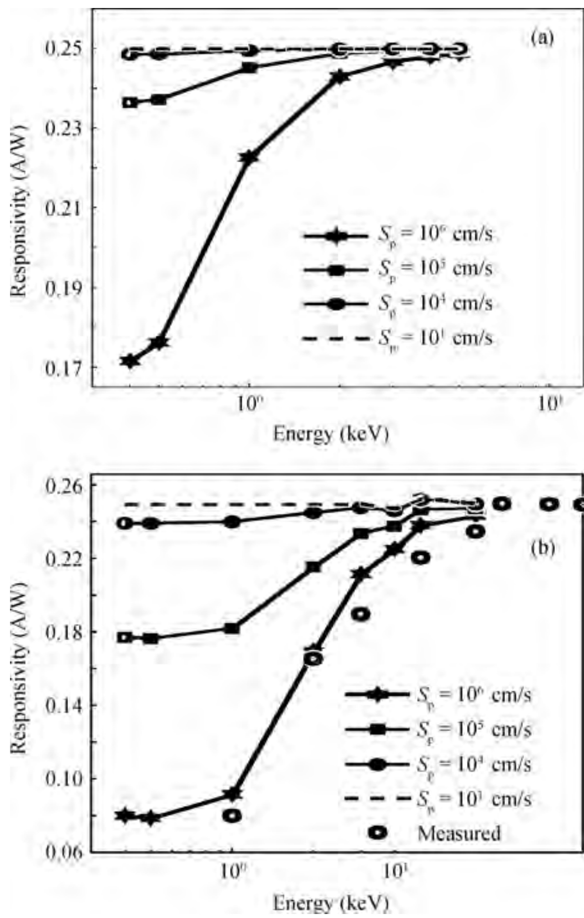

Fig. 5. Influence of interface recombination velocity of minority carriers on the responsivity of (a) arsenic doped n^+p detector, (b) phosphorus doped n^+p detector from 400 to 8 keV where $Q_f = 5 \times 10^{11}$ cm^{-2}. This value of Q_f was chosen because typical values for Q_f are in the order of 10^{10}–10^{11} charges per cm^{-2}, depending on the process conditions[4]. Also research has shown that for some interfaces, the magnitude of the fixed charge can be up to 10^{12} cm^2 (one-hundredth of the interface atoms) especially under interface bond strain and bias voltage applied to the detector oxide[15, 16].

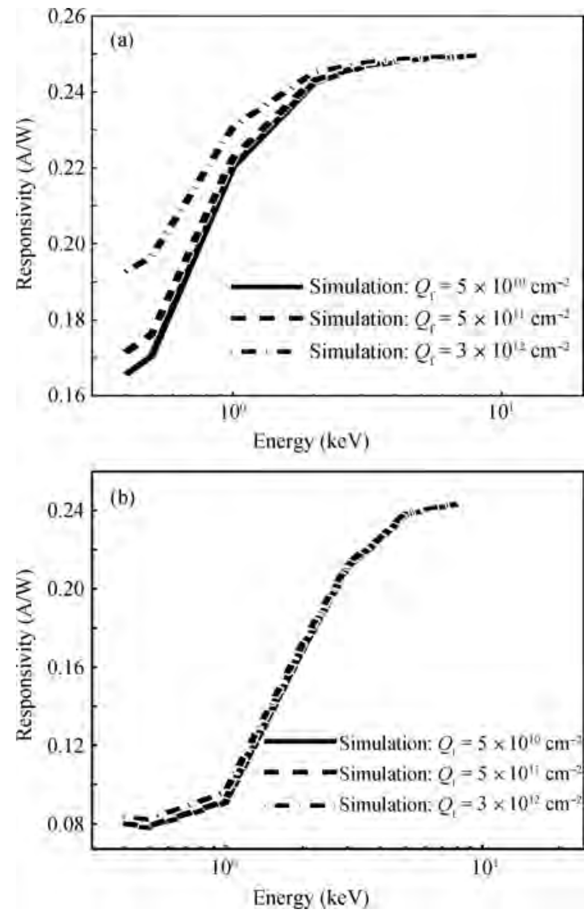

Fig. 6. Simulation result of the effect of fixed oxide charge, Q_f on (a) arsenic doped n^+p detector and (b) phosphorus doped n^+p detector where $S_p \approx 10^6$ cm/s on the responsivity in amps/watts from 400 to 8 keV.

ties[4] δ_r (A/W) of the detector as defined in Eq. (3). A faraday cup was first irradiated with an electron beam of energy v_o to measure the beam current I_o which was used to determine the quantity of electrons hitting the cup.

The detector was then irradiated with a beam containing the same number of electrons and the resulting current I_{pd} was measured with the use of a digital ammeter as shown in Fig. 4(a). The average of several measured I_o values was used for statistical accuracy. Current–voltage measurements were done to ascertain the detector's leakage current in comparison with the simulated detectors and the results are shown in Fig. 4(b).

As a result of the relatively high dark current, the SEM measurement was done on the detector without detector bias voltage to minimise the adverse effect of leakage current on the result. δ_r is defined as

$$\delta_r = \frac{I_{pd}}{P} = \frac{I_{pd}}{I_o v_o}, \tag{3}$$

where I_{pd} is the measured detector current; P is the beam power; I_o, the incident beam current; and v_o, the electron acceleration voltage.

3.2. Results

The effect of interface recombination velocity of minority carriers and fixed oxide charge on the responsivity of the simulated and measured detectors are shown in Figs. 5 and 6, with the maximum responsivity observed to be approximately 0.25 A/W. The responsivities of the detectors in Fig. 5 were achieved with different interface recombination velocities of minority carriers S_p present at the Si–SiO_2 interface at a constant fixed oxide charge, Q_f of a typical silicon material.

As shown in Fig. 5, at a constant Q_f and at each given interface recombination velocity and energy, the responsivity of the n^+p detector doped with arsenic is about 0.17 A/W and 0.24 A/W at 0.5 keV and 2 keV, respectively, while the phosphorus doped detector is 0.08 A/W and 0.17 A/W for the same energies. The difference between the responsivity from both detectors is not unexpected as the doping profile of both detectors is different, as seen in Fig. 2. What this implies is that

[4]Without any recombination, 0.27 A/W is expected with an average of 3.6 eV per electron-hole pair used.

the responsivity of a detector could be influenced by the doping concentration or the profile of dopant impurities. The difference may also be due to the dissociation effect and anomalous behaviour exhibited by phosphorus diffusion in silicon, even though its diffusion in silicon is associated with a doubly charge acceptor vacancy V^{2-}[3].

The result from the measured detector in Fig. 5(b) is seen to agree with the simulation and this can implicitly give us an idea of the fixed oxide charge and the surface recombination velocity values of the detector. As such the detector can be said to have an approximate values of 5×10^{11} cm^{-2} of fixed oxide charge and interface recombination velocity of 10^6 cm/s.

From Fig. 5, it is seen that the measured electrical output per optical input cannot be significantly improved even when the interface recombination velocity is reduced to less than 10^4 cm/s. The n^+p detector doped with arsenic exhibits the traits of a perfectly responsive detector at an interface recombination velocity of approximately 10^4 cm/s whereas it would take a slightly lower interface recombination velocity for the phosphorus doped n^+p detector to display such characteristic. This implies that even when there is a substantial interface recombination velocity at the oxide–silicon interface of up to 10^4 cm/s, the arsenic doped n^+p detector and phosphorus doped n^+p detector will still exhibit near maximum responsivity of 0.25 A/W in this case. It also means that when the interface recombination velocity is $\leqslant 10^4$ cm/s there is no electron energy loss to processes that do not lead to the creation of electron–hole pairs.

A similar result obtained at each energy from Fig. 5 can also be noticed in Fig. 6. At a constant S_p, the result as depicted in Fig. 6 shows that the responsivity of the detectors saturates at a similar energy when the fixed oxide charge Q_f is varied. One significant difference is that the phosphorus doped n^+p detector can be described as being slightly more suppressive or resistive to the influence of Q_f.

4. Conclusion

We have, through this research, been able to explore an alternative method of characterizing an n^+p doped detector under electron irradiation. We have also been able to use the measure of the electrical output per optical input in the form of electrons to infer the interface recombination velocity and fixed oxide charge present in an n^+p detector. We were able to obtain the maximum responsivity of both the simulated and measured detector (as 0.25 A/W in this research) using our method and the result is in agreement with those obtained from previous studies[14].

We were able to use a new method devised as an alternative to known standard methods to characterize the surface state properties of the detector. The method was successfully used to investigate the level of the input–output gain, the surface recombination velocity and fixed oxide charges present at an n^+p detector interface using a scanning electron microscope.

References

[1] Jin H. Relationship between interface defect density and surface recombination velocity in (111) and (100) silicon/silicon oxide structure. 23rd European Photovoltaic Solar Energy Conference, 2008: 244
[2] Langer J M, Walukiewicz W. Surface recombination in semiconductors. Materials Science Forum, 1995, 196–201: 1389
[3] Sze S M. Physics of semiconductor devices. 3rd ed. New Jersey: John Wiley Interscience, 2007
[4] May G S, Sze S M. Fundamentals of semiconductor fabrication. John Wiley & Sons, 2004: 53
[5] Hesler J L, Crowe T W. NEP and responsivity of THz zero-bias Schottky diode detectors. Joint 32nd International Conference on Infrared and Millimeter Waves, and the 15th International Conference on Terahertz Electronics, 2007: 844
[6] Buda M. Characterization of high performance PbS photodetectors. J Optoelectron Adv Mater, 2008, 10(2): 306
[7] Funsten H O, Suszcynsky D M, Ritzau S M, et al. Response of 100% internal quantum efficiency silicon photodiodes to 200 eV-40 keV electrons. IEEE Trans Nucl Sci, 1997, 44(6): 2561
[8] Moldovan G, Kazemian P, Edwards P R, et al. Low-voltage cross-sectional EBIC for characterization of GaN-based light emitting devices. Ultramicroscopy, 2007, 107(4/5): 382
[9] Parish C, Batchelor D, Progl C, et al. Electron beam-induced current in the scanning electron microscope. Microscopy and Analysis, 2007, 21(5): 11
[10] CERN. Geant4 scope of application. 2011
[11] Grove A S. Physics and technology of semiconductor devices. New York: John Wiley & Sons, 1967
[12] Caughey D M, Thomas R E. Carrier mobilities in silicon empirically related to doping and field. Proc IEEE, 1967, 55(12): 2192
[13] Cuevas A, Basore P A, Giroult-Matlakowski G, et al. Surface recombination velocity of highly doped n-type silicon. J Appl Phys, 1996, 80(6): 3370
[14] Korde R, Geist J. Quantum efficiency stability of silicon photodiodes. Appl Opt, 1987, 26(24): 5284
[15] Szekeres A, Simeonov S, Gushterov A, et al. Electrical properties of plasma-assisted CVD deposited thin silicon oxynitride films. J Optoelectron Adv Mater, 2005, 7(1): 553
[16] Bera M K, Maiti C K. Electrical properties of SiO_2/TiO_2 high-k gate dielectric stack. Materials Science in Semiconductor Proceeding, 2006, 9(6): 909